Available online at www.sciencedirect.com

ScienceDirect

Ceramics International 40 (2014) 1321–1328

CERAMICS INTERNATIONAL

www.elsevier.com/locate/ceramint

Morphological, structural, and gas-sensing characterization of tin-doped indium oxide nanoparticles

A. Ayeshamariam[a,*], M. Kashif[b], M. Bououdina[c,d], U. Hashim[b], M. Jayachandran[e], M.E. Ali[f]

[a]Department of Physics, Khadir Mohideen College, Adirampattinam 614701, India
[b]Nano Biochip Research Group, Institute of Nano Electronic Engineering (INEE), Universiti Malaysia Perlis (UniMAP), Kangar 01000, Perlis, Malaysia
[c]Nanotechnology Centre, University of Bahrain, PO Box 32038, Bahrain
[d]Department of Physics, College of Science, University of Bahrain, PO Box 32038, Bahrain
[e]ECMS Division, Central Electro Chemical Research Institute (CSIR), Karaikudi 630004, India
[f]Nanotechnology and Catalysis Research Centre, University of Malaya, Kuala Lumpur 50603, Malaysia

Received 19 June 2013; received in revised form 22 June 2013; accepted 1 July 2013
Available online 20 July 2013

Abstract

Tin-doped indium oxide (ITO) nanoparticles with stable cubic phases were synthesized using a sol–gel combustion method that includes gelation and combustion in organic fuel. The influence of SnO_2 on the phase and morphology of the In_2O_3 nanoparticles were studied by X-ray diffraction, scanning electron microscopy, and high resolution transmission electron microscopy (TEM), along with selected area electron diffraction. ITO nanoparticles with 11–20 nm crystallite size and 69–46 m^2/g specific surface area were obtained. The lattice constant was nearly 10.12 Å, with orientation along the (222), (400), and (110) planes for all proportions of the doped SnO, indicating a stable cubic phase with high conductivity. The TEM micrograph of the ITO nanoparticles and powder revealed spherical morphology. The microstructure of the cured In_2O_3: Sn with Sn concentrations of 5, 10, 20, and 50 wt% demonstrated that the ITO nanoparticles clustered more densely with the increase in Sn concentration. The gas-sensing ability of the synthesized powders was demonstrated through the sensing of ethanol vapor at 200 °C.

Keywords: Sol–gel combustion; Sn-doped indium oxide; Structural; Electrical

1. Introduction

Tin-doped indium oxide (ITO) powder/films have been used to manufacture transparent conductive coatings. ITO is an advanced semiconducting material with potential applications in touch panel contacts, electrodes for LCD/electro-chromic displays, defogging aircraft windows, gas sensors, and antistatic window coatings [1–4]. Research and development studies on ITO have been focused on the synthesis and properties of its powder [1–3]. Different forms of ITO powder with low-dimensional and quasi-one-dimensional structured semiconducting particles, such as nanosphere [5], nanocircle [6], nanorod [2], nanowire [7], and nanotube [8], have been of great technological interest for devices requiring larger surface areas. However, high electrical conductivity is observed only in the stable cubic phase [9–11]. Various methods are available for preparing ITO powder, such as co-precipitation [5,12], vapor–liquid–solid [13], sol–gel [14], and emulsion techniques [8,15]. The high electrical conductivity property of ITO is caused by the creation of a conducting carrier-oxygen vacancy with the addition of the dopant (Sn) within the In_2O_3 matrix.

Sol–gel combustion is a novel method, with a unique combination of both the chemical sol–gel technique and the combustion process [16]. This method is based on the gelation and subsequent combustion of an aqueous solution containing salts of the desired metals and organic fuel such as urea, which leads to a voluminous and fluffy product with large surface area. This process offers several advantages, including inexpensive precursors, a simple preparation method, a final output of nanosized powder, and so on. The present study investigates the possibility of obtaining ITO nanopowder with a uniform particle size through the sol–gel combustion process.

*Corresponding author. Tel.: +91 9486738806.
E-mail address: aismma786@gmail.com (A. Ayeshamariam).

0272-8842/$ - see front matter © 2013 Elsevier Ltd and Techna Group S.r.l. All rights reserved.
http://dx.doi.org/10.1016/j.ceramint.2013.07.012

When Sn is added above the solubility limit, metastable secondary phases may appear to form a new composite material. However, detailed studies on the behavior of Sn on substitution in nanocrystalline ITO powder with a wide range of Sn^{4+} content above the solubility limit have not been performed. In this study, ITO powder with various levels of Sn content was synthesized by sol–gel combustion. The structural and micro-structural characterization of the nanocrystalline ITO powder were examined and reported. Gas-sensing measurements were carried out on ethanol vapor.

2. Experimental

Powders of In_2O_3:Sn with various Sn concentrations were prepared through sol–gel combustion. $Sn(NO_3)_2 \cdot 5H_2O$ (99.99%), $In(NO_3)_3 \cdot 7H_2O$ (99.99%), and NH_2CONH_2 (50%) were purchased from Sigma-Aldrich and used without further purification. In and Sn solutions were prepared by dissolving 4.752 g of $In(NO_3)_3 \cdot 7H_2O$ and 0.648 g of $Sn(NO_3)_2 \cdot 5H_2O$ in 20 mL of deionized (DI) water, respectively. The quantity of the metal ions in the solution was adjusted to achieve the final ratio of ternary oxide (In_2O_3/SnO_2) at 95:05, 90:10, 80:20, and 50:50. An aqueous urea solution was prepared by dissolving 0.4 g of urea in 10 mL of DI water. The prepared urea solution was then added dropwise to the In/Sn solution under constant stirring until a sol was formed. The bath temperature was maintained at 30 °C. This sol was heated at 120 °C for 20 min and then placed in a muffle furnace for 20 min until a dry gel was obtained. The samples were then ignited in a furnace at 350 °C, in which an auto-combustion process occurred, and a burnt powder was formed. The obtained burnt powder was subsequently calcined at 400 °C for 1 h.

The structural properties of the ITO nanoparticles were investigated using an X-ray diffractometer (Model Philips Expert Pro). The X-ray diffraction (XRD) pattern was recorded in the range of 10° to 80°, operating at a voltage of 40 kV and a current of 40 mA. Morphological studies were performed using scanning electron microscopy (SEM) with a Hitachi S-3400 N. Structural analysis was carried out by transmission electron microscopy (TEM) using a 200 kV Tecnai-20 G2 TEM instrument. The selected area electron diffraction (SAED) pattern was also recorded. Gas-sensing measurements were carried out in a chamber comprising a vacuum coating unit, a temperature controller, and a Keithley 2000 multifunction meter.

For the measurement of gas sensitivity, the sensing elements based on ITO nanocrystalline powders were fabricated in a conventional manner [10]. The powders were pressed into pellets under a pressure of 15 MPa and then Al lead was mounted on both sides of the pellet to form the sensing element. The gas sensing measurements were carried out in a static chamber with a volume of 25 L. The operating temperature of the sensor was measured by adjusting the current flow through the heater, and temperature was controlled using a Cr–Al thermocouple. Sensor sensitivity was defined as follows:

$$s = \left(\frac{R_{vac} - R_{gas}}{R_{gas}}\right) \quad (1)$$

Resistance was measured by the half-bridge technique [17]. The operating temperature of the ethanol sensor was optimized for the highest response of the test gas. The optimized temperature was tested for 1000 ppm of ethanol.

3. Results and discussion

Fig. 1(a–d) shows the XRD patterns of the ITO powders containing 5%, 10%, 20%, and 50% SnO_2 annealed at 400 °C. The result suggested that the crystallinity of the In_2O_3 powders decreased with dopant concentrations. All ITO powder particles showed preferred orientation along the (222) direction. The relative intensity of the (222) peak decreased with increasing Sn concentration [18]. Particles with adequate energy were oriented along a thermodynamically favorable (222) direction. As the concentration of In_2O_3 decreased, the energy of the doped particles increased, and the particles moved more actively toward thermodynamically stable sites.

The observed (d) values matched perfectly with that of the cubic lattice of JCPDS standard card no. 89-4598. No additional peaks corresponding to additional phases were observed; hence, no impurities existed. This result indicates that the ITO phase formation was completed during the combustion process. Notably, a single phase material was obtained through the solid-state reaction route only after prolonged calcinations of the reaction mixture at relatively high temperatures with multiple intermediate grindings.

The particle size was determined by the X-ray line broadening method using Scherer's equation:

$$D = \frac{0.94\lambda}{\beta \cos\theta} \quad (2)$$

where D is the particle size, λ is the wavelength of the X-ray radiation source (1.5406 Å for Cu-Kα radiation), β is the corrected peak full width at half-maximum, and θ is the peak position. The calculated values of the crystallite size are listed in Table 1.

The crystallite size of the as-prepared powders varied slightly with increasing Sn content (Fig. 2a) within the range of 11–20 nm. Similarly, the crystallite size increased slightly within a very narrow limit with increasing annealing temperature. Small amounts of Sn (up to 5% Sn) cause a decrease in the lattice constant, thereby leading to a decrease in bond length. As the Sn content increases, the bond length slowly increases due to the distortion of In–Sn–O. This distortion increases the lattice constant (Fig. 2b) and decreases the crystal density of the crystal structures. Fig. 2c shows the peak intensity ratio of the (222)/(440) planes for various Sn concentrations. The peak intensity ratio decreases with decreasing Sn concentration. The lattice constants and bond lengths, crystallite size, and crystalline density were calculated, and the refinement values are shown in Table 2. The variation in bond length, which increases at the tetrahedral site and decreases at the octahedral site of the ITO powder obtained in 50:50 proportions, may be attributed to the relative value of occupancy of In to Sn at the site.

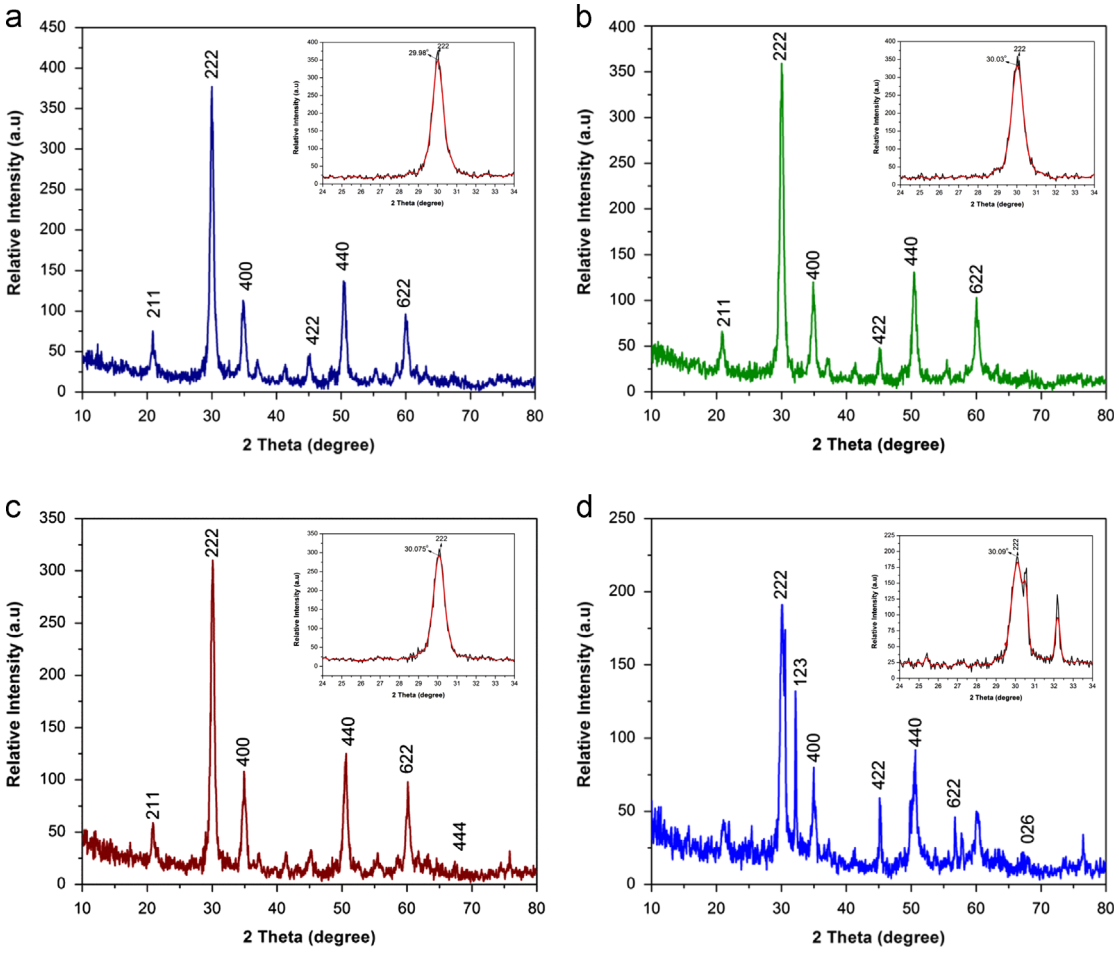

Fig. 1. XRD pattern of Indium oxide nanoparticles are 5% (a) 10% (b), 20% (c) and 50% (d) of SnO_2/In_2O_3 annealed at 400 °C.

Table 1
Crystalline size of 5%, 10%, 20%, and 50% of $SnO_2/In2O_3$ powders.

$D = (0.94\lambda)/(\beta \cos\theta)$, (nm)	ITO (95:05)	ITO (90:10)	ITO (80:20)	ITO (50:50)
400 °C	15.290	14.981	16.562	23.92

The isotropic microstrain introduced within the crystal lattice may be associated with the variation in the ionic radii of the substituting cations (Sn^{2+} occupying In^{2+}). The microstrain change causes the distortion of the bond length as well. Minimum microstrains are observed at 5% Sn. With further increase of Sn amount, the lattice defects also increase. The microstrains of the various concentrations were calculated based on the ionic radii of In^{2+} and Sn^{2+}.The different ratios of the (222)/(440)-oriented grains in this study can also lead to the variation of the surface area. Table 3 shows that the surface area depends on the particle size.

ITO powders with higher intensity ratios exhibit higher mobility and lower resistivity. The ITO powder with growth direction along the (222) plane accommodates larger amount of interstitial oxygen atoms into the powdered particles because of the non-uniform distribution of oxygen vacancies. The (222) ITO of 5 wt% of Sn shows a smaller density of free electrons compared with that of the 50 wt% of particles synthesized by the combustion process because the interstitial oxygen atoms extinguish free electrons when combined with the substituting Sn^{2+} ions. Hence, the preparation of ITO nanopowder with higher density of free electrons must involve acceleration of the crystalline growth along the (222) orientation.

The bixbyite structure of In_2O_3 contains 80 atoms in a conventional cell and 40 atoms in the primitive unit cell. In_2O_3 has two in equivalent In sites [In-8b (1/4, 1/4, 1/4), labeled as In1 and In-24d (u,0, 1/4), labeled as w In2] and one in the equivalent O site [O-48e (*x*,*y*,*z*) in the Wyckoff notation]. Both In1 and In2 are sixfold-coordinated surrounded by O atoms, whereas all the O atoms are fourfold-coordinated surrounded by In atoms. The conventional cell of In_2O_3 in the bixbyite structure and the calculated local structures are shown in Fig. 3(a–d).

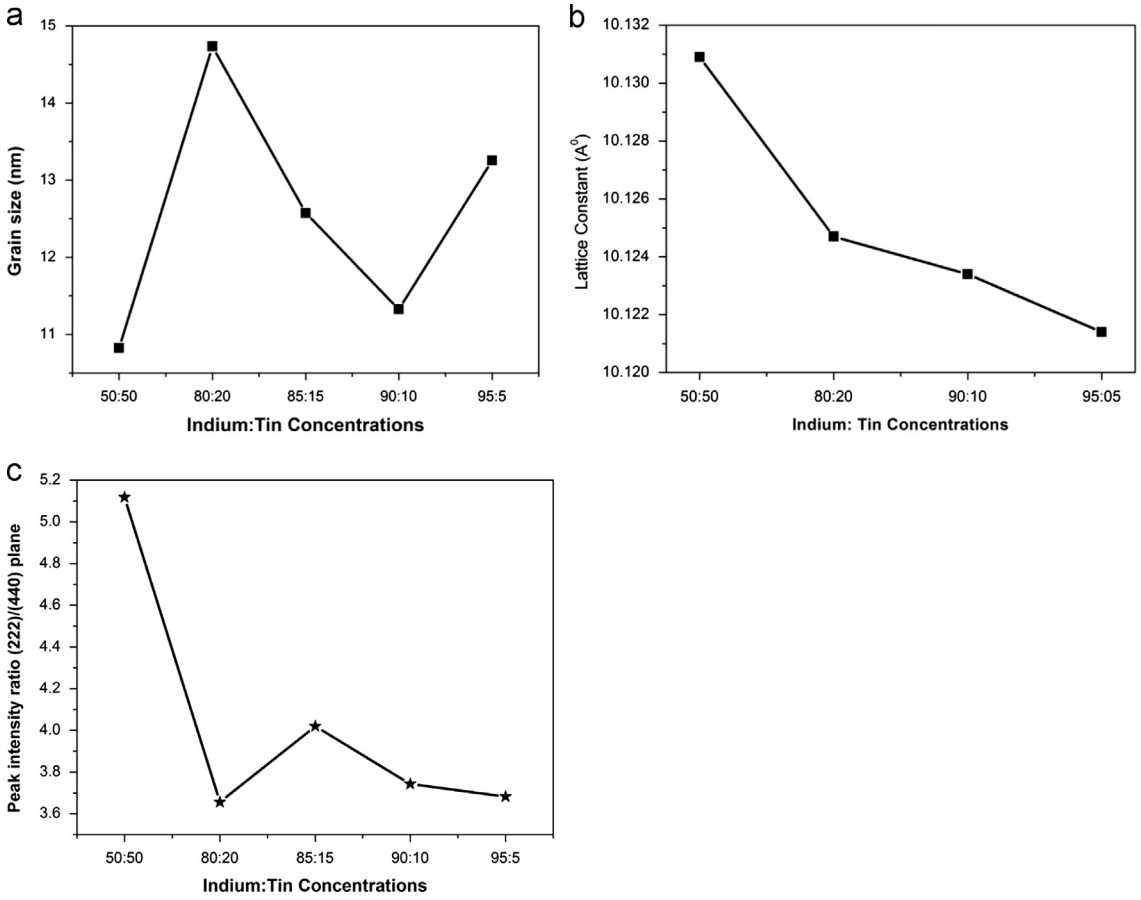

Fig. 2. (a) Grain size, (b) lattice constant and (c) peak intensity ratios of In_2O_3 with different Sn% concentrations.

Table 2
Structural parameters of 5%, 10%, 20%%, and 50% of $SnO_2/In2O_3$ powders.

Parameters	$In_{95}Sn_{05}$	$In_{90}Sn_{10}$	$In_{80}Sn_{20}$	$In_{50}Sn_{50}$
R_{wp}	8.06	8.61	9.48	9.60
R_p	5.99	6.42	7.38	7.54
R_{Bragg}	1.043	1.055	1.126	1.020
GOF	1.06	0.81	0.76	0.77
SpaceGroup	Ia-3(206)	Ia-3(206)	Ia-3(206)	Ia-3(206)
$a=b=c$ (Å)	10.1214	10.1234	10.1247	10.1309
Volume (A^3)	1036.86	1037.48	1037.88	1039.79
$\alpha=\beta=\gamma$	90	90	90	90
Crystallite size (nm) (Lorentzian)	11.621	12.212	15.120	19.03
Crystal density (g/cm^3)	6.510	6.180	6.196	6.106

Table 3
Surface area of 5%, 10%, 20%, and 50% of $SnO_2/In2O_3$.

$S=6/\rho D$, m^2/g	ITO (95:05)	ITO (90:10)	ITO (80:20)	ITO (50:50)
400 °C	60.27855	64.80701	58.46919	41.0734

The local structure of In1 is highly symmetric, and all six In–O–Sn bonds have the same length (slightly smaller than the average value of all In–O–Sn bonds). For the oxygen vacancy (V_O) in the neutral charge state, an O atom appeared from an otherwise perfect crystal, leaving two electrons in a defect state, which is a symmetrical combination of the four In dangling bonds.

Fig. 4 shows the SEM images of the In_2O_3 powders comprising different concentrations of SnO_2, with 5%, 10%,

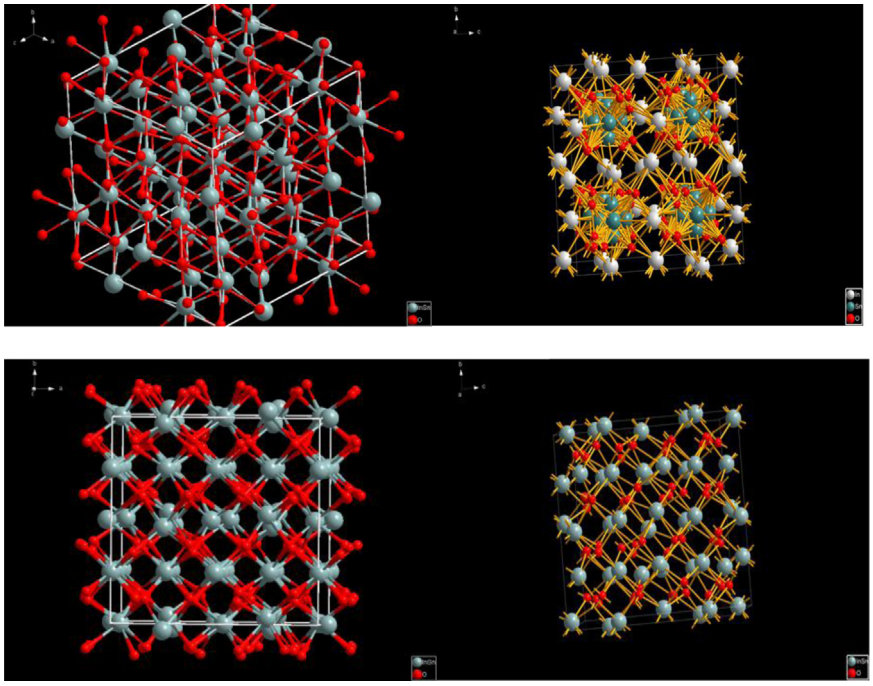

Fig. 3. Arrangement of Sn, In and O atoms in unit cells of 5% (a) 10% (b), 20% (c) and 50% (d) of SnO_2/In_2O_3.

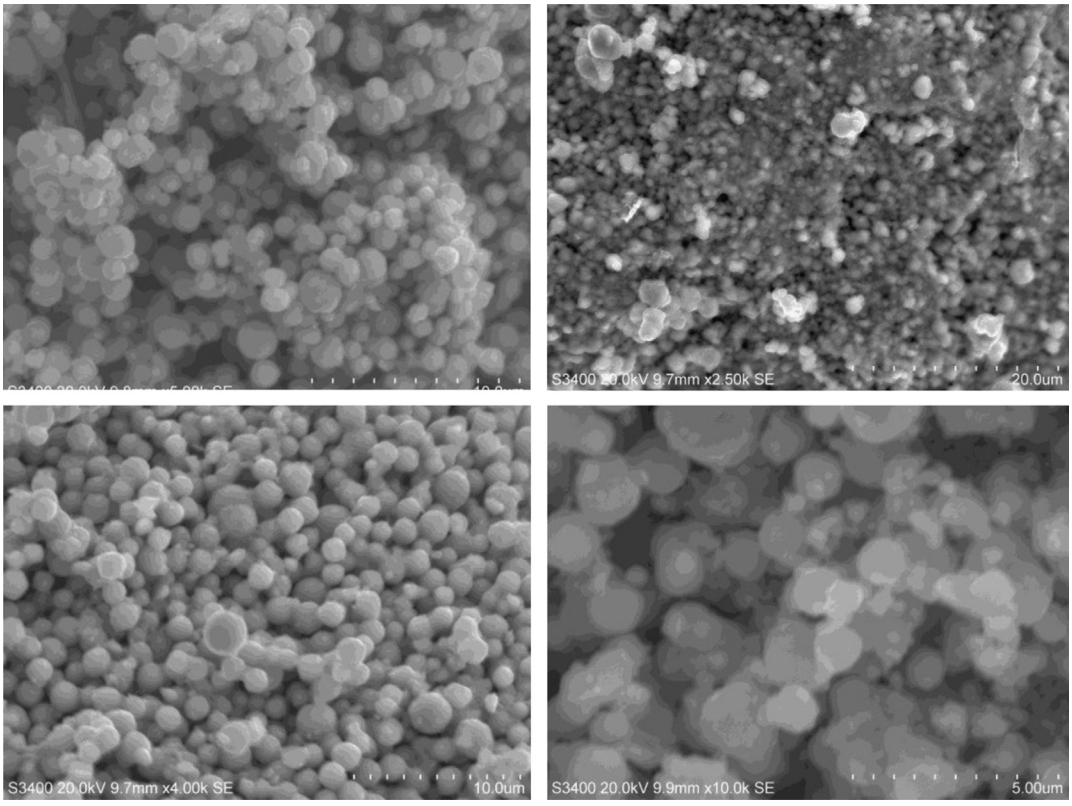

Fig. 4. SEM images of Sn doped ITO nanoparticles are 5% (a) 10% (b), 20% (c) and 50% (d) of SnO_2/In_2O_3 annealed at 400 °C.

20% and 50% for (a), (b), (c), and (d), respectively. Grain sizes and shapes were observed by SEM, and dense granular structures were observed. The grains have different shapes and sizes. The value of the grain size obtained using SEM is larger than that derived from XRD. Each spherical grain is composed of very minute crystallites of nano-dimension. The intensity of Sn reaction with In_2O_3 determines the grain morphology, and results show that they are individually

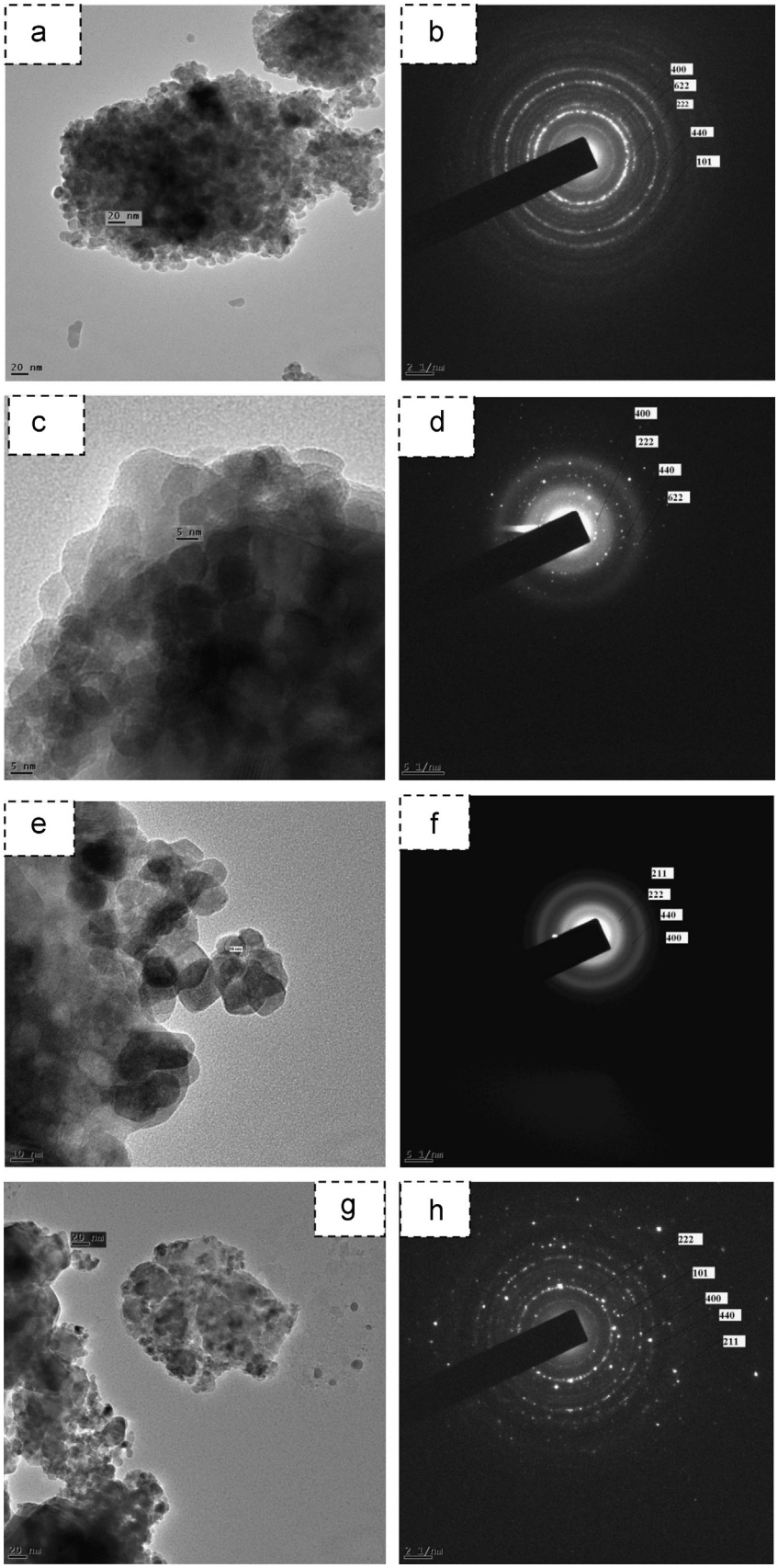

Fig. 5. TEM images and SAED patterns of Sn doped In_2O_3 are 5% (a) 10% (b), 20% (c) and 50% (d) of SnO_2/In2O_3.

observed as spherical particles. This result confirms the large specific surface area of ITO powders prepared in the present study, which is a useful property required for sensor applications. The surface area of the particles affects grain agglomeration.

TEM images and related observations of the nanograined ITO powder with various Sn% content are shown in Fig. 5. The particle size increases with increasing Sn content, as visually inspected from the bright-field images of the powders. Similarly, particle agglomeration increases with increasing Sn content. The above result agrees with the observations obtained from the SEM study. The SAED patterns presented in Fig. 5(b, d, f, and h) confirm that the sol–gel combustion-prepared In_2O_3:Sn powder exhibits a cubic structure, confirming the incorporation of Sn within the original In_2O_3 crystal lattice. The observed strong rings show the formation of highly nanocrystalline grains in the powder.

The peaks observed are the same as those observed in XRD (Fig. 1a). High-resolution TEM (HRTEM) images of the powders showed lattice fringes from which (222), (400), and (110) planes were observed. The tendency of grain size increase with Sn content was in good agreement with the results obtained from XRD (Fig. 1d) and SEM (Fig. 4d). Thus, the sol–gel combustion technique can be used for the preparation of ITO nanoparticles with controlled size and various Sn contents.

Fig. 6 shows the sensitivity–temperature behavior of 1000 ppm of ethanol at different ITO ratios. The sensitivity reached the maximum value at 200 °C for all the samples and then decreased with further increase in temperature.

The Al electrodes placed on the surface of the pellet displayed an ohmic behavior. Initially, the chamber was evacuated to a base pressure of 10^{-2} Torr using a rotary pump. The temperature was controlled by varying the current flow through the heater, measured with an accuracy of 1 °C using a temperature controller with indicator. After noting the reference response, the test gas was injected into the bell jar through a

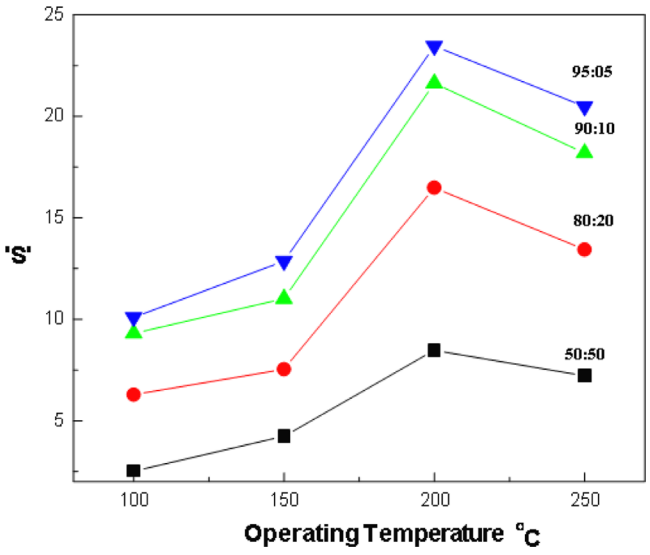

Fig. 6. Sensitivity curve as a function of temperature at different Sn doped In_2O_3 nanoparticles.

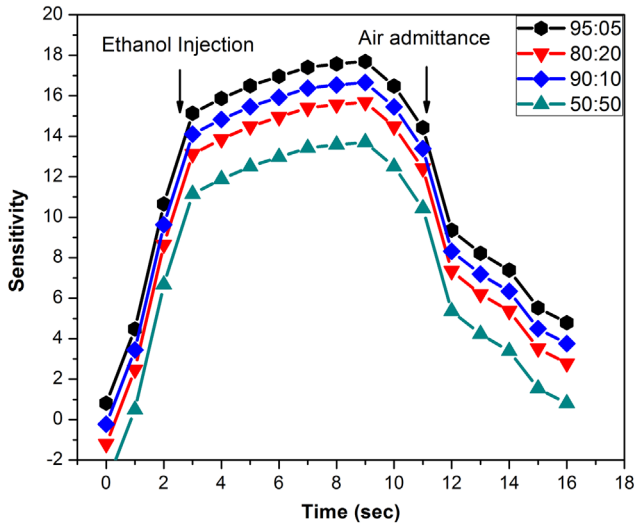

Fig. 7. Time response curve of Sn doped of In_2O_3 for 1000 ppm ethanol concentration at 200 °C.

needle valve. After injecting the test gas (in this case, ethanol), all the valves were closed to avoid leakage. The resistance of the sensor was again measured at the same temperature in ambient ethanol vapor. After collecting the measurements, the gas was cleared by injecting fresh air into the chamber to carry out the next cycle.

Fig. 7 shows the variation of sensitivity and response time with annealing temperature. The response time reaches a maximum at 2 min, and then recovers within 4 min. The sensitivity is higher for the powder with smaller particle size, and the response time increases with larger particle size [19].

The presence of ethanol gas causes the transfer of electronic charge at the surface, which primarily depends on both gas concentration and temperature [20]. Given that In_2O_3:Sn nanoparticles are *n*-type semiconductors with oxygen vacancies that generally provide donor states, the conductivity of the In_2O_3:Sn nanoparticles is directed by the steady concentration of adsorbed oxygen ions and determined by chemical dynamics, including oxidation and diffusion [21]. The surface of In_2O_3:Sn reacts faster with negatively charged oxygen adsorbates, resulting in water and free electrons. As a result, the sensitivity of In_2O_3:Sn nanoparticles increases and remains constant, as shown in Fig. 7.

In the case of metal oxide semiconductors, intrinsic conductance increases with increasing temperature, whereas adsorbed oxygen molecules transform into oxygen ions (O^-, O_2^-, O^{2-}) by capturing free electrons from the oxide, thereby causing a decrease in conductance of the oxide with increasing temperature. At temperatures between 100 and 500 °C, the adsorption of oxygen leads to ionized molecular ($O^-_{2(ads)}$) or atomic species ($O^-_{(ads)}$, $O^-_{2(ads)}$), depending on the temperature. The reaction kinetics can be described as follows [22]:

$$O_{2(ads)} \leftrightarrow O^-_{2(ads)} \leftrightarrow 2O^-_{(ads)} \leftrightarrow 2O^{2-}_{(ads)} \quad (3)$$

The adsorbed oxygen molecules capture free electrons from the conduction band and form oxygen ions according to the

following formula:

$$O_{2(ads)} + 2e^- \leftrightarrow 2O^-_{(ads)} \quad (4)$$

Depletion layers were formed on the surface regions, causing the carrier concentration to decrease. When the sensor is exposed to ethanol vapor, ethanol molecules as reducing gas will react with oxygen ions on the surface of the TIO particles. The reaction is given by [23,24]:

$$CH_3CH_2OH_{(ads)} + 6O_{2(ads)} \rightarrow 2CO_2 + 3H_2O + 6e^- \quad (5)$$

The electrons are released back to the conduction band, ultimately increasing the sensor current.

4. Conclusion

ITO nanoparticles with stable cubic phase were synthesized through sol–gel combustion. The particles had a diameter of 11–20 nm with spherical morphology and 69–46 m^2/g specific surface area. The lattice constant was nearly 10.12 Å oriented along the (222), (400), and (110) planes, indicating a stable cubic phase with high conductivity. The gas-sensing properties of the ITO particles were studied in an airtight chamber with 1000 ppm of ethanol vapor. The gas-sensing sensitivity increased with increasing operating temperature up to 200 °C and then decreased. The maximum sensitivity occurred at 200 °C irrespective of the ethanol concentration. The sensor showed moderate response and recovery time.

References

[1] H.R. Xu, H. Zhou, G. Zhu, J. Chen, C. Liao, Synthesis of tin-doped indium oxide nanoparticles by an ion-exchange and hydrothermal process, Materials Letters 60 (2006) 983.

[2] S.J. Limmer, K. Takahashi, G. Cao, Synthesis of indium tin oxide (ITO) and fluorine-doped tin oxide (FTO) nano-powder by sol–gel combustion hybrid method, Proceedings of the SPIE—The International Society for Optical Engineering 5224 (2003) 25.

[3] J. Hu, F. Zhu, J. Zhang, H. Gong, A room temperature indium tin oxide/quartz crystal microbalance gas sensor for nitric oxide, Sensors and Actuators B 93 (2003) 175.

[4] A. Antony, M. Nisha, R. Manoj, M.K. Jayaraj, Effect of substrate temperature on the growth of ITO thin films, Applied Surface Science 225 (2004) 294.

[5] M. Biswas, K. Shashidhara, P.K. Ojha, T.K. Chon-gdar, Linear combination of atomic orbitals approximation in nanocrystalline yittria-stabilized zirconia synthesized by citrate–nitrate gel combustion process, Journal of the American Ceramic Society 91 (3) (2008) 934–937.

[6] N.G. Patel, P.D. Patel, V.S. Vaishnav, Indium tin oxide (ITO) thin film gas sensor for detection of methanol at room temperature, Sensors and Actuators B 96 (2003) 180.

[7] M.J. Alam, D.C. Cameron, Investigation of an nealing effects on sol–gel deposited indium tin oxide thin films in different atmospheres, Thin Solid Films 420–421 (2002) 76.

[8] K.Y. Kim, S.B. Park, Preparation and property control of nano-sized indium tin oxide particle, Materials Chemistry and Physics 86 (2004) 210.

[9] S.G. Chen, C.H. Li, W.H. Xiong, L.M. Liu, H. Wang, Synthesis of indium tin oxide (ITO) and fluorine-doped tin oxide (FTO) nano-powder by sol–gel combustion hybrid method, Materials Letters 58 (2004) 294.

[10] D. Yu, D. Wang, W. Yu, Y. Qian, Synthesis of ITO nanowires and nanorods with corundum structure by a co-precipitation-anneal method, Materials Letters 58 (2003) 84.

[11] H. Zhu, Y. Wang, N. Wang, Y. Li, J. Yang, Hydrothermal synthesis of indium hydroxide nanocubes, Materials Letters 58 (2004) 2631.

[12] P.S. Devi, M. Chatterjee, D. Ganguli, P.S. Devi, M. Chatterjee, D. Ganguli, Indium tin oxide nano-particles through an emulsion technique, Materials Letters 55 (2002) 205–210.

[13] T. Peng, X. Liu, K. Dai, J. Xiao, H. Song, Effect of acidity on the glycine-nitrate combustion synthesis of nanocrystalline alumina powder, Materials Research Bulletin 41 (9) (2006) 1638–1645.

[14] N.C. Pramanik, S. Das, Biswas, The effect of Sn (IV) on transformation of co-precipitated hydrated In (III) and Sn (IV) hydroxides to indium tin oxide (ITO) powder, Materials Letters 56 (2002) 671–679.

[15] D. Yu, D. Wang, W. Yu, Y. Qian, Synthesis of ITO nanowires and nanorods with corundum structure by a co-precipitation-anneal method, Materials Letters 58 (2003) 84.

[16] R.D. Purohit, S. Saha, A.K. Tyagi, Combustion synthesis of nanocrystalline ZrO_2 powder: XRD, Raman spectroscopy and TEM studies, Materials Science and Engineering: B 130 (1–3) (2006) 57–60.

[17] P. Siciliano, Preparation, characterisation and applications of thin films for gas sensors prepared by cheap chemical method, Sensors and Actuators B 70 (2000) 153–164.

[18] Y.S. Jung, S.S. Lee, Development of indium tin oxide film texture during dc magnetron sputtering deposition, Journal of Crystal Growth 259 (2003) 343.

[19] Z. Zhan, J. Lu, W. Song, D. Jiang, J. Xu, Highly selective ethanol In_2O_3-based gas sensor, Materials Research Bulletin 42 (2007) 228.

[20] J. Zhang, J.Q. Hu, F.R. Zhu, H. Gong, S.J. Oshea, ITO thin films coated quartz crystal microbalance as gas sensor for NO detection, Sensors and Actuators B 87 (2002) 159–167.

[21] C. Baratto, G. Faglia, E. Comini, G. Sberveglieri, A. Taroni, V. La Ferrara, L. Quercia, G. Di Francia, A novel porous silicon sensor for detection of sub-ppm NO_2 concentrations, Sensors and Actuators B: Chemical 77 (2001) 62.

[22] V. Brinzari, G. Korotcenkov, J. Schwank, V. Lantto, S. Saukko, V. Golovanov, Morphological rank of nano-scale tin dioxide films deposited by spray pyrolysis from $SnCl_4 \cdot 5H_2O$ water solution, Thin Solid Films 408 (2002) 51.

[23] V.S. Vaishnav, P.D. Patel, N.G. Patel, Indium Tin Oxide thin film gas sensors for detection of ethanol vapours, Thin Solid Films 490 (2005) 94.

[24] A. Ayeshamariam, M. Bououdina, C. Sanjeeviraja, et al., Optical, electrical and sensing properties of In2O3 nanoparticles, Material Science in Semiconducting Processing 16 (3) (2013) 686–695.